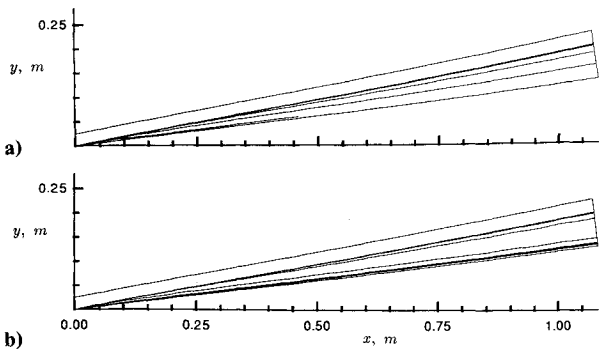

Fig. 3 Flow over a 7-deg cone with an adiabatic boundary layer: a) pressure contours, b) density contours.

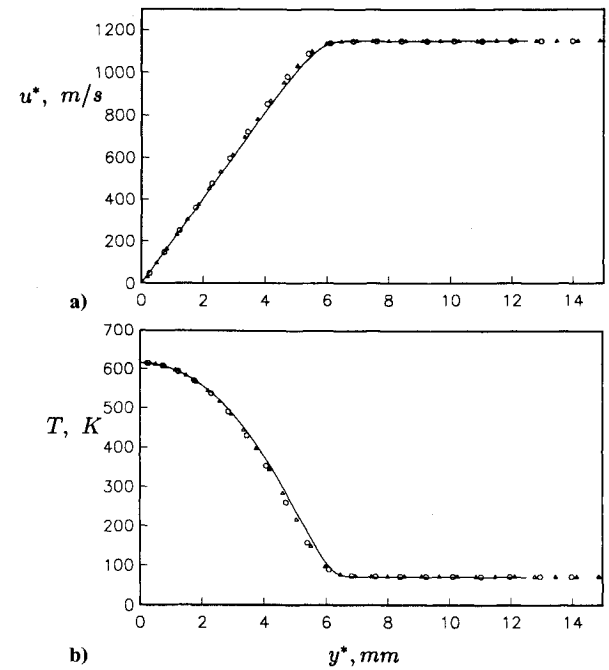

Fig. 4 Comparison of the present finite volume solution with a spectral solution at 1.0 m from the cone apex: a) tangential velocity, b) temperature. Solid line represents spectral solution, o denotes 100 × 60 mesh, △ denotes 100 × 90 mesh.

B. Flow over a Sharp Cone

To illustrate the behavior of the solver in the presence of strong viscous effects, we show the computed results for $M \simeq 8$ flow over a sharp 7-deg cone. The axis of the cone is aligned with the freestream.

Two cases are considered in which the cone flow domain is discretized as a set of 100×60 cells and 100×90 cells. Freestream conditions of $\rho = 1.0809 \times 10^{-2}$ kg/m^3, $P = 165.51$ Pa, $e = 3.8281 \times 10^4$ J/kg, $T = 53.35$ K, $u = 1164.0$ m/s, $v = 0$, and $M_{\text{nominal}} = 7.95$ are applied to the left and upper boundaries whereas the outflow boundary conditions are obtained by extrapolation, and the cone surface is modeled as a no-slip, adiabatic boundary. To match the experimental conditions in Ref. 11, the gas was considered to be a perfect gas with $\gamma = 1.4$, $R = 287$ J/kg/K, and $Pr = 0.7$, and viscosity was obtained from the Sutherland expression

$$\mu = 1.611 \times 10^{-6} \frac{T^{3/2}}{T + 110.33} \text{ Pa.s}$$

Based on freestream conditions and the length of the cone, the Reynolds number is approximately 3.3×10^6. The initial state of the flow in the domain is $\rho = 1.0809 \times 10^{-2}$ kg/m^3, $P = 165.51$ Pa, $e = 3.8281 \times 10^4$ J/kg, $u = 0$, and $v = 0$. The Navier-Stokes equations are then integrated forward in time using high-order MUSCL interpolation and Euler time stepping with a CFL number of 0.5.

Figure 3 shows the flowfield (pressure and density contours) $t = 22$ ms after the flow has approached steady state. The pressure field is almost conically symmetric, as per the inviscid solution of Taylor and Maccoll (see for example, Chap. 10 in Ref. 12), and the shock angle is still approximately the inviscid value of 10.5 deg (Ref. 9, Chart 4). The shock, however, is slightly curved near the apex of the cone. Boundary-layer profiles of velocity and temperature at $x^* = 1.0$ m are shown in Fig. 4 for both the present finite volume solutions and a boundary-layer solution using edge conditions of $\rho_e = 2.044 \times 10^{-2}$ kg/m^3, $P_e = 416.7$ Pa, $u_e^* = 1148.6$ m/s, and $T_e = 71.04$ K. There is good agreement between the present finite volume solutions and the spectrally accurate solution,[13] especially near the cone surface. Although the outer region of the boundary layer is underresolved (even for the 100×90 mesh), the finite volume solutions appear to be converging to the spectral solution.

References

[1]Gottlieb, J. J., and Groth, C. P. T., "Assessment of Riemann Solvers for Unsteady One-Dimensional Inviscid Flows of Perfect Gases," *Journal of Computational Physics,* Vol. 78, No. 2, 1988, pp. 437–458.

[2]Roe, P. L., "Approximate Riemann Solvers, Parameter Vectors, and Difference Schemes," *Journal of Computational Physics,* Vol. 43, No. 2, 1981, pp. 357–372.

[3]Osher, S., and Solomon, F., "Upwind Difference Schemes for Hyperbolic Systems of Conservation Laws," *Mathematics of Computation,* Vol. 38, No. 158, 1982, pp. 339–374.

[4]Quirk, J. J., "An Adaptive Grid Algorithm for Computational Shock Hydrodynamics," Ph.D. Thesis, College of Aeronautics, Cranfield Inst. of Technology, Bedford, England, UK, 1991.

[5]Peery, K. M., and Imlay, S. T., "Blunt-Body Flow Simulations," AIAA Paper 88-2904, 1988.

[6]Godunov, S. K., (ed.), *Numerical Solution of Multidimensional Problems in Gasdynamics,* Nauka, Moscow, 1976.

[7]Jacobs, P. A., "Single-Block Navier-Stokes Integrator," Inst. for Computer Applications in Science and Engineering, ICASE Interim Rept. 18, NASA Langley Research Center, Hampton, VA, July 1991.

[8]Billig, F. S., "Shock-Wave Shapes Around Spherical- and Cylindrical-Nosed Bodies," *Journal of Spacecraft and Rockets,* Vol. 4, No. 6, 1967, pp. 822, 823.

[9]Ames Research Staff, "Equations, Tables and Charts for Compressible Flow," NACA Rept. 1135, 1953.

[10]White, J., NASA Langley Research Center, private communication, 1991.

[11]Stetson, K. F., Thompson, E. R., Donaldson, J. C., and Siler, L. G., "Laminar Boundary Layer Stability Experiments on a Cone at Mach 8, Part 1: Sharp Cone," AIAA Paper 83-1761, 1983.

[12]Anderson, J. D., *Modern Compressible Flow: with Historical Perspective,* McGraw-Hill, New York, 1982.

[13]Pruett, C. D., and Streett, C. L., "A Spectral Collocation Method for Compressible, Nonsimilar Boundary Layers," *International Journal for Numerical Methods in Fluids,* Vol. 13, No. 6, 1991, pp. 713–737.

Grid Studies for Thin-Layer Navier-Stokes Computations of Airfoil Flowfields

D.W. Zingg*

University of Toronto Institute for Aerospace Studies, Toronto, Ontario M3H 5T6, Canada

Introduction

THE status of computational methods for viscous transonic airfoil flows is reviewed in detail in Ref. 1, which

Received Oct. 29, 1991; presented as Paper 92-0184 at the AIAA 30th Aerospace Sciences Meeting, Reno, NV, Jan. 6–9, 1992; revision received Feb. 19, 1992; accepted for publication March 30, 1992.

*Assistant Professor, 4925 Dufferin Street, Downsview, Ontario. Member AIAA.

summarizes the results of the "Viscous Transonic Airfoil Workshop," in which several groups applied a variety of numerical procedures to a specified set of transonic flow cases. The results of the workshop show that for transonic attached flows lift is generally predicted to within ± 3% and drag to within ± 5% of the experimental values. For separated flows, the errors can be considerably larger.

Errors in the computation of steady viscous airfoil flows can result from two sources: numerical errors and physical-model errors. Numerical errors include spatial discretization errors associated with inadequate grid clustering and refinement and further errors associated with the position of the outer boundary. Physical models that are subject to error include the thin-layer approximation and other approximations in the governing equations, prediction of the transition point and the process of transition, and the turbulence model. Further complications are introduced by experiments used for comparisons, which are also subject to error, unsteadiness, and three dimensionality.

The purpose of this Note is to evaluate numerical errors for a range of flow cases and to reduce them to reasonable levels. This is accomplished through numerical solution-to-solution comparisons including grid-refinement studies and outer boundary-position studies. Error estimates are obtained using Richardson extrapolation, as in Ref. 2. In addition to providing useful guidelines for determining the levels of grid refinement and the outer boundary position required to achieve a given level of accuracy, the grid-independent solutions obtained provide an accurate evaluation of physical-model errors. Further details of the present study are included in Ref. 3.

Numerical Algorithm and Error Estimates

The thin-layer Navier-Stokes equations are solved numerically using the viscous transonic airfoil code ARC2D, which is described in detail in Ref. 4. Spatial derivatives are approximated using second-order centered finite difference expressions. The now standard nonlinear artificial dissipation model, which combines second- and fourth-difference dissipation, is used to control oscillations and nonlinear instability. No-slip adiabatic conditions are enforced at the airfoil surface. Characteristic boundary conditions are used at outer boundaries. In addition, a far-field circulation correction is applied at the outer boundary. The Baldwin-Lomax turbulence model is used to compute the eddy viscosity.

Estimates of global truncation error can be obtained using the Richardson extrapolation technique described by Zingg.[2] Given an initial grid (grid A), a coarser grid (grid B) is found by removing every second point in each curvilinear coordinate direction. Since the spatial discretization is second-order accurate, improved estimates of lift and drag can be obtained by combining the solutions computed on the two grids in the following manner:

$$C_{l_{AB}} = \frac{(4C_{l_A} - C_{l_B})}{3}, \qquad C_{d_{AB}} = \frac{(4C_{d_A} - C_{d_B})}{3} \tag{1}$$

Therefore, estimates of the truncation error in the lift and drag coefficients computed on grid A are given by

$$\Delta C_{l_A} = \frac{(C_{l_B} - C_{l_A})}{3}, \qquad \Delta C_{d_A} = \frac{(C_{d_B} - C_{d_A})}{3} \tag{2}$$

Results and Discussion

Computational results are presented for the following six cases:

1) NACA 0012 at $M_\infty = 0.16$, $\alpha = 0$ deg, $Re = 2.88 \times 10^6$, transition at 0.43 chords on both surfaces.

2) NACA 0012 at $M_\infty = 0.16$, $\alpha_{corr} = 6$ deg, $Re = 2.88 \times 10^6$, transition at 0.05 and 0.8 chords on the upper and lower surfaces, respectively.

3) NACA 0012 at $M_\infty = 0.16$, $\alpha_{corr} = 12$ deg, $Re = 2.88 \times 10^6$, transition at 0.01 and 0.95 chords on the upper and lower surfaces, respectively.

4) NACA 0012 at $M_\infty = 0.7$, $\alpha_{corr} = 1.49$ deg, $Re = 9 \times 10^6$, transition at 0.05 chords.

5) NACA 0012 at $M_\infty = 0.55$, $\alpha_{corr} = 8.34$ deg, $Re = 9 \times 10^6$, transition at 0.05 chords.

6) RAE 2822 at $M_{\infty corr} = 0.729$, $\alpha_{corr} = 2.31$ deg, $Re = 6.5 \times 10^6$, transition at 0.03 chords.

The subsonic cases were previously computed by Mehta et al.[5] and were studied experimentally by Gregory and O'Reilly.[6] For these cases, the transition points correspond to the measured values on a clean airfoil given in Ref. 6. The transonic flow conditions correspond to cases from the Viscous Transonic Airfoil Workshop.[1] Experimental data for these cases are given in Refs. 7 and 8. They were originally studied using ARC2D by Maksymiuk and Pulliam[9] and were revisited by Maksymiuk et al.[10] with somewhat more refined grids. The angle-of-attack and Mach number corrections for the transonic cases correspond to those used by Maksymiuk et al.[10]

Results are presented for several grids, all of which have a "C" type topology and were generated using the hyperbolic grid generator described in Ref. 11. For both airfoils, the grids designated "A7A" have 497 × 193 points with 401 points on the body and 48 points in the wake. Points are clustered at the leading and trailing edges with a spacing of 0.0001 chords. The distance to the outer boundary is 12 chords. Normal spacing at the body is 10^{-7} chords. Grid W7A has 297 × 321 points with 241 points on the body and 28 points in the wake. Clustering is the same as grid A7A except that the clustering near the trailing edge is 0.001 chords. The grids designated "N7A" have 497 × 97 points with the same clustering as grids A7A. Grid N6A is identical to grid N7A except that the normal spacing at the body is 10^{-6} chords. Grids A7B, W7B, N7B, and N6B were produced by removing every second point from grids A7A, W7A, N7A, and N6A, respectively.

Results for the subsonic cases are shown in Tables 1-3. These include a nonlifting case, a case at moderate lift with fully attached flow, and a case at higher lift with separation predicted at roughly 96% chord on the upper surface. The solutions labeled "AB" were obtained using Richardson extrapolation. The measured lift and drag coefficients are given at the bottom of each table. The columns labeled "%" show the truncation error estimates except in the row labeled "experiment" where they show the difference between the measured values and those obtained on grid W7A. In Table 1, the individual drag components, pressure drag C_{d_p} and friction drag C_{d_f}, are also presented. Lift and drag are generally converged to the accuracy shown in the tables.

Table 1 Grid-refinement study for the NACA 0012 airfoil at $M_\infty = 0.16$ and $\alpha = 0$ deg

Grid	Size	C_d	C_{d_p}	C_{d_f}	%C_d
A7A	497 × 193	0.00584	0.00081	0.00503	0.9
A7B	249 × 97	0.00600	0.00085	0.00514	3.6
A7AB		0.00579	0.00080	0.00499	—
N7A	497 × 97	0.00595	0.00087	0.00508	3.8
N7B	249 × 49	0.00660	0.00113	0.00547	15.2
N7AB		0.00573	0.00078	0.00495	—
N6A	497 × 97	0.00626	0.00085	0.00541	11.7
N6B	249 × 49	0.00823	0.00105	0.00717	47.0
N6AB		0.00560	0.00078	0.00482	—
W7A	297 × 321	0.00604	0.00083	0.00521	0.5
W7B	149 × 161	0.00614	0.00087	0.00526	2.2
W7AB		0.00601	0.00082	0.00519	—
Experiment		0.0069			−12.5

Table 2 Grid-refinement study for the NACA 0012 airfoil at $M_\infty = 0.16$ and $\alpha = 6$ deg

Grid	Size	C_l	C_d	%C_l	%C_d
A7A	497 × 193	0.6614	0.00798	−0.09	2.4
A7B	249 × 97	0.6597	0.00856	−0.3	9.9
A7AB		0.6620	0.00779	—	—
N7A	497 × 97	0.6580	0.00836	−0.2	7.9
N7B	249 × 49	0.6539	0.01018	−0.8	31.4
N7AB		0.6594	0.00775	—	—
W7A	297 × 321	0.6674	0.00790	0.2	1.2
W7B	149 × 161	0.6705	0.00818	0.6	4.7
W7AB		0.6664	0.00781	—	—
Experiment		0.650	0.0094	2.7	−16.0

Table 3 Grid-refinement study for the NACA 0012 airfoil at $M_\infty = 0.16$ and $\alpha = 12$ deg

Grid	Size	C_l	C_d	%C_l	%C_d
A7A	497 × 193	1.3081	0.01327	−0.3	5.2
A7B	249 × 97	1.2957	0.01526	−1.3	21.0
A7AB		1.3122	0.01261	—	—
N7A	497 × 97	1.2991	0.01455	−0.8	15.8
N7B	249 × 49	1.2673	0.02049	−3.2	63.0
N7AB		1.3097	0.01257	—	—
W7A	297 × 321	1.3170	0.01294	−0.08	3.4
W7B	149 × 161	1.3142	0.01420	−0.3	13.4
W7AB		1.3179	0.01252	—	—
Experiment		1.240	0.0180	6.2	−28.1

For case 1, transition was fixed at 0.40 chords for grids W7A and W7B and at 0.43 chords for the other grids. This was done in order to maintain the same transition point on the fine and coarse grids used in obtaining the error estimates. For this case, the solution obtained on grid N6A has a much higher friction drag error than the solution obtained on grid N7A. For grid N6A the first point off the body corresponds to a y^+ value of less than 0.2 around the entire airfoil while for grid N7A the corresponding y^+ value is less than 0.02. Thus grid N6A provides an adequately fine spacing at the surface. The increased friction drag error is associated with inadequate resolution in the outer portion of the boundary layers.

The generally good agreement between the drag coefficient obtained by Richardson extrapolation on different grids indicates that the error estimates are quite accurate. In all three subsonic cases, grid W7A produces the smallest numerical error, although for case 3 the numerical error in drag remains large considering that the grid contains roughly 95,000 nodes. The comparisons of the solutions obtained on grid W7A with experiment show that the physical-model errors are very large, even when the flow is attached. In some cases, grids which lead to higher numerical error, such as grid N6A, produce better agreement with the experimental drag coefficient, potentially leading to false conclusions regarding the accuracy of the physical models.

Results for the transonic cases are shown in Tables 4–6. In these tables, the values in the columns labeled "%" listed beside the experimental data give the difference between the measured values and those obtained on grid A7A. Computed and experimental pressure distributions for these cases are compared in Refs. 1, 9, and 10, generally showing good agreement.

For case 4, the computations predict a weak shock on the upper surface but the flow remains fully attached. Grid N6A again produces a much larger friction drag error than grid N7A. Case 5 has a strong shock on the upper surface at about 20% chord. There is a small separated flow region after the shock and the flow finally separates at about 90% chord. Case 6 has a shock on the upper surface, a small separated flow region after the shock, and trailing-edge separation at 98% chord. For all three transonic cases, grid A7A leads to numerical errors in lift and drag which are less than 1%.

Table 4 Grid-refinement study for the NACA 0012 airfoil at $M_\infty = 0.7$ and $\alpha = 1.49$ deg

Grid	Size	C_l	C_d	%C_l	%C_d
A7A	497 × 193	0.2538	0.00747	0.08	0.5
A7B	249 × 97	0.2545	0.00760	0.4	2.3
A7AB		0.2536	0.00743	—	—
N7A	497 × 97	0.2536	0.00749	−0.3	1.2
N7B	249 × 49	0.2515	0.00775	−1.1	4.7
N7AB		0.2543	0.00740	—	—
N6A	497 × 97	0.2534	0.00774	−0.2	5.2
N6B	249 × 49	0.2517	0.00888	−0.9	20.7
N6AB		0.2540	0.00736	—	—
Experiment		0.241	0.0079	5.3	−5.4

Table 5 Grid-refinement study for the NACA 0012 airfoil at $M_\infty = 0.55$ and $\alpha = 8.34$ deg

Grid	Size	C_l	C_d	%C_l	%C_d
A7A	497 × 193	0.9977	0.03484	−0.4	0.2
A7B	249 × 97	0.9868	0.03509	−1.4	0.9
A7AB		1.0013	0.03476	—	—
N7A	497 × 97	0.9955	0.03519	−0.4	1.7
N7B	249 × 49	0.9835	0.03698	−1.6	6.9
N7AB		0.9995	0.03459	—	—
Experiment		0.983	0.0253	1.5	37.5

Table 6 Grid-refinement study for the RAE 2822 airfoil at $M_\infty = 0.729$ and $\alpha = 2.31$ deg

Grid	Size	C_l	C_d	%C_l	%C_d
A7A	497 × 193	0.7937	0.01346	−0.2	0.7
A7B	249 × 97	0.7898	0.01375	−0.7	2.9
A7AB		0.7950	0.01336	—	—
N7A	497 × 97	0.7908	0.01360	−0.4	2.0
N7B	249 × 49	0.7803	0.01440	−1.8	8.0
N7AB		0.7943	0.01333	—	—
Experiment		0.743	0.0127	6.8	6.0

Physical-model errors are very large for the transonic cases as well. For case 4, which has a weak shock, the computations overestimate the lift and underestimate the drag, as in the subsonic cases. For the remaining transonic cases, which have stronger shocks, the computations overestimate the drag.

Results of the outer boundary-position studies are presented in Table 7. For each airfoil, an initial grid was generated with the outer boundary located at roughly 96 chords. Smaller grids were then generated by removing the outer grid lines from this initial grid. Therefore, the effect of the outer boundary position can be studied separately from grid-resolution effects. In Table 7, the columns labeled "%" show the difference from the value computed with the outer boundary at 96 chords. The results show that an outer boundary position of 12 chords produces very little error in lift. The error in drag is somewhat larger, with the largest error occurring for the subsonic case at high lift. For this case, the grid with the outer boundary located at 12 chords underestimates the drag by 3.4% relative to the grid with the outer boundary at 96 chords. However, increasing the outer boundary distance to 24 chords reduces this error to 1.5%.

The grid requirements for a given case are dependent on the spatial discretization, the artificial dissipation scheme, and the turbulence model used. Upwind schemes and centered schemes with matrix artificial dissipation would be expected to have

Table 7 Results of outer boundary-position studies

Case	Grid	Outer boundary	C_l	C_d	$\%C_l$	$\%C_d$
1	493 × 192	96 chords	—	0.00610	—	—
	455 × 170	12	—	0.00610	—	0.0
2	493 × 192	96	0.6655	0.00818	—	—
	455 × 170	12	0.6672	0.00805	0.3	−1.6
3	493 × 192	96	1.3111	0.01397	—	—
	469 × 178	24	1.3121	0.01376	0.08	−1.5
	455 × 170	12	1.3139	0.01349	0.2	−3.4
4	493 × 192	96	0.2569	0.00748	—	—
	455 × 170	12	0.2571	0.00747	0.06	−0.1
5	493 × 192	96	1.0039	0.03546	—	—
	455 × 170	12	1.0040	0.03542	0.01	−0.1
6	493 × 192	96	0.7990	0.01376	—	—
	455 × 171	12	0.7980	0.01359	−0.1	−1.2

reduced grid-resolution requirements.[12] Consequently, the conclusions which can be drawn from the present results apply strictly only to second-order centered difference schemes which use the scalar dissipation model described in Ref. 4 with the Baldwin-Lomax turbulence model. The results of the outer boundary-position studies also reflect the boundary-condition treatment used in ARC2D, including the far-field circulation correction. However, the results obtained provide useful guidelines for other flow solvers and turbulence models as well as a systematic approach for assessing their grid requirements.

Conclusions

A detailed investigation of the effects of grid clustering and refinement on the prediction of lift and drag in thin-layer Navier-Stokes computations of viscous airfoil flowfields has been presented. The effect of the location of the outer boundary of the grid has been examined as well. The flow cases studied exhibit a variety of flow features. The results can be summarized as follows. Grids W7A and A7A, which contain roughly 95,000 nodes, lead to spatial discretization errors of less than 1% in both lift and drag for most of the subsonic and transonic cases, respectively. Numerical errors of less than 1 % in lift only are obtained in all cases using grids N7A and N6A, which have roughly 48,000 nodes. Grid W7B, with roughly 24,000 nodes, produces less than 1% errors in lift for the subsonic cases. An outer boundary position of 12 chords introduces virtually no error in lift. Somewhat larger distances to the outer boundary are required to reduce the associated error in drag to below 1%. These results provide useful guidelines for determining the levels of grid refinement and the outer boundary position required to achieve a given level of accuracy for a range of flow conditions. The relatively grid-independent solutions obtained also provide an accurate assessment of the errors associated with the physical models used.

References

[1]Holst, T. L., "Viscous Transonic Airfoil Workshop Compendium of Results," AIAA Paper 87-1460, Honolulu, HI, June 1987.

[2]Zingg, D. W., "Viscous Airfoil Computations Using Richardson Extrapolation," AIAA Paper 91-1559, Honolulu, HI, June 1991.

[3]Zingg, D. W., "Grid Studies for Thin-Layer Navier-Stokes Computations of Airfoil Flowfields," AIAA Paper 92-0184, Reno, NV, Jan. 1992.

[4]Pulliam, T. H., "Efficient Solution Methods for the Navier-Stokes Equations," *Lecture Notes for the Von Karman Institute for Fluid Dynamics Lecture Series: Numerical Techniques for Viscous Flow Computation in Turbomachinery Bladings,* Von Karman Inst. for Fluid Dynamics, Brussels, Belgium, Jan. 20–24, 1986.

[5]Mehta, U., Chang, K. C., and Cebeci, T., "Relative Advantages of Thin-Layer Navier-Stokes and Interactive Boundary-Layer Procedures," NASA TM 86778, Nov. 1985.

[6]Gregory, N., and O'Reilly, C. L., "Low-Speed Aerodynamic Characteristics of NACA 0012 Airfoil Section, Including the Effects of Upper-Surface Roughness Simulating Hoar Frost," Aeronautical Research Council, Reports and Memoranda No. 3726, U.K., Jan. 1970.

[7]Harris, C. D., "Two-Dimensional Aerodynamic Characteristics of the NACA 0012 Airfoil in the Langley 8-Foot Transonic Pressure Tunnel," NASA TM 81927, April 1981.

[8]Cook, P. H., MacDonald, M. A., and Firmin, M. C. P., "Aerofoil RAE 2822—Pressure Distributions, and Boundary-Layer and Wake Measurements," AGARD-AR-138, May 1979.

[9]Maksymiuk, C. M., and Pulliam, T. H., "Viscous Transonic Airfoil Workshop Results Using ARC2D," AIAA Paper 87-0415, Reno, NV, Jan. 1987.

[10]Maksymiuk, C. M., Swanson, R. C., and Pulliam, T. H., "A Comparison of Two Central Difference Schemes for Solving the Navier-Stokes Equations," NASA TM-102815, July 1990.

[11]Barth, T. J., Pulliam, T. H., and Buning, P. G., "Navier-Stokes Computations for Exotic Airfoils," AIAA Paper 85-0109, Reno, NV, Jan. 1985.

[12]Swanson, R. C., and Turkel, E., "On Central-Difference and Upwind Schemes," Institute for Computer Applications in Science and Engineering, ICASE Rept. 90-44, Hampton, VA, June 1990.

Effect of Streamwise Pressure Gradient on the Supersonic Mixing Layer

Takashi Abe* and Katsushi Funabiki†
Institute of Space and Astronautical Science, Kanagawa 229, Japan
Hironobu Ariga‡
Musashi Institute of Technology, Tokyo 158, Japan
and
Katsumi Hiraoka§
Tokai University, Kanagawa 259-12, Japan

Introduction

THE mixing process in supersonic flow attracts much attention in scramjet engine research.[1] Extensive studies by not only experimental methods[2–4] but also by theoretical and numerical methods[5] have focused on this field. Among them, Papamoschou and Roshko[3] examined the compressibility effect on the mixing layer at the interface of the parallel supersonic flows and clarified the fact that the growth rate of the mixing layer is reduced by the compressibility effect in comparison with the one without the compressibility effect. In their study the mixing process was examined by means of the flow visualization technique by schlieren photography. Recently several researchers concentrated on enhancing the growth rate of the supersonic mixing layer,[4,5] since, e.g., the enhancement of mixing implies the improvement of the performance of the scramjet engine. In the present Note we attempt to clarify the effect of the streamwise pressure gradient of the flow on the growth rate of the mixing layer formed at the interface of the parallel supersonic flows. For this purpose the structure of the mixing layer was examined by the in-site measurement of the concentration ratio of the gas mixture.

Received July 16, 1991; revision received April 7, 1992; accepted for publication April 13, 1992.

*Associate Professor, Division of Space Transportation, Yoshinodai 3-1-1, Sagamihara. Member AIAA.

†Research Assistant, Division of Space Transportation.

‡Graduate Student, School of Engineering.

§Associate Professor, School of Engineering. Member AIAA.